Shrinkage evaluation and geometric accuracy assessment on 17–4 PH samples made by material extrusion additive manufacturing

(Article begins on next page)

11 February 2025

Shrinkage evaluation and geometric accuracy assessment on 17-4 PH samples made by Material Extrusion Additive Manufacturing

Abstract: Material Extrusion Additive Manufacturing (MEX) is one of the most common Additive Manufacturing (AM) technology. The possibility to realize metal parts using this technology has several advantages and generates great costs reduction with respect to other metal Additive Manufacturing technologies. However, there are some disadvantages related to the design and production of these extrusion-based metal parts, especially when considering the fabrication of complex geometries. One of the main problems is related to the oversizing of the parts due to the shrinkage phenomenon occurring after the debinding and sintering steps.

In this work, a comprehensive study about the shrinkage phenomenon was conducted on 17-4 PH stainless steel parts realized via MEX, analyzing the influence of printing and sintering orientation, infill strategy and aspect ratio. With this aim, by using the Design of Experiment approach, samples were analyzed in both as-printed and as-sintered conditions. Shrinkage percentage values, geometric accuracy and density were the main investigated outputs. A commercial 3D structured-light scanner was used to collect the dimensional and geometric data.

Results showed a strong shrinkage anisotropy, more relevant for samples with different orientation during the printing and the sintering phase. Geometric accuracy, in terms of flatness, was also assessed comparing green and sintered parts.

Keywords: MEX, 17-4 PH, shrinkage, geometric accuracy, sintering.

1. Introduction

The rapidly growing Additive Manufacturing (AM) has simplified the fabrication of complex and customized shapes manufactured using different metals such as stainless steels, copper, titanium alloys and aluminum alloys [1]. When applied to metals, AM is named Metal Additive Manufacturing (MAM) [2]. MAM may provide environmental advantages such as less wastage, less pollutant emissions, quality improvement and the possibility to make parts on demand [3,4]. Although, the extent of utilization of these technologies in industry is currently limited to a few sectors, such as dental, automotive, and aerospace. The main MAM are referred to powder bed fusion (PBF) technologies like Selective Laser Melting (SLM), Electron Beam Melting (EBM) and Direct Metal Laser Sintering (DMLS) [5]. SLM, EBM and DMLS are the most commercially employed processes, but they still have some limitations. These processes are very expensive as they need an inert

atmosphere and/or vacuum to avoid oxidation and they require high energy sources. Material handling is also critical and special equipment is required for storage, handling and eventually recycling, with relevant health and safety issues [6]. Recently, an economic and simple alternative has been identified in metal-composite filament extrusion processes based on Material Extrusion Additive Manufacturing (MEX) technology. In literature, when the feedstock material is in a filament form, the process of metal MEX takes different names, e.g. Fused Deposition of Metal (FDMet) [7], Fused Deposition Modeling and Sintering (FDMS) [8], or Metal Fused Filament Fabrication (Metal FFF) [9]. In these cases, filaments, which can be both commercial or made in laboratory, can be processed by consumer MEX machines and the system architecture is mainly open. On the other hand, Atomic Diffusion Additive Manufacturing (ADAM) is a patented MEX technology characterized by a very similar process chain, which uses proprietary feedstock materials and equipment. This hybrid technique, based on MEX and Metal Injection Molding (MIM) processes, uses a mixture of metal powder and different binders as material feedstock. The binder part can be divided in a main component (50-90 vol.%), a backbone binder (10-50 vol.%) and some additives (1-10 vol.%) [10]. Being a MIM-based technology, the required process chain, necessary to obtain a full metal part without remnants of binder, consists of two other phases after printing: Debinding and Sintering (D&S). Debinding enables the removal of polymers from the green part since carbon residues can influence the sintering process and can affect the quality of the final product in a negative way [11]. Sintering, with a proper combination of time and temperature, burns the polymeric part residual and densifies the metallic powder. As rule, sintering is performed at temperatures below the melting temperature of the major constituent in powder, generally within 70 to 90% of the powder's melting point [10]. Thus, to ensure that a part is complete and suitable for a certain function, the entire process chain needs to be fulfilled. The volume and weight loss occurring during the debinding and sintering phases makes necessary the oversizing of the part to compensate the shrinkage occurring after the D&S. The choice of the proper oversizing factor is related to the debinding and sintering treatments for the realization of the final part.

1.1   *Research background*

The shrinkage is one of the main problems for hybrid metal process as MIM and metal MEX. In the literature, the shrinkage is often investigated as a "collateral" aspect, while most of the interest is focused on the mechanical performance or microstructural aspects of the sintered parts. Although, the shrinkage evaluation is a fundamental aspect of the investigated process chain, especially in the perspective of using this technology for the fabrication of complex geometries, where even small geometric variations with respect to the nominal characteristics lead to significant variations in terms of structural properties [12]. When the shrinkage is discussed, it is generally related to the parameters

of debinding and sintering and the building orientation of the printed parts. Léonard and Tammas-Williams [13] analyzed the shrinkage rate for 17-4 PH parts realized by Atomic Diffusion Additive Manufacturing (ADAM) using X-ray computed tomography and confirmed the anisotropy of this phenomenon. Sung et al. [14] found a linearity between shrinkage and sintering temperature on 17-4 PH parts realized by MIM. Singh et al. [15] evaluated the effect of sintering temperature on shrinkage and density by analyzing 17-4 PH cylinders fabricated by using a MIM feedstock. They confirmed that, increasing the sintering temperature, the shrinkage increases, and samples become denser. Heaney and Spina [16] studied the shrinkage on MIM carbonyl iron (61.1 vol%) samples during the two subsequent debinding steps (solvent and thermal) and pre-sintering and sintering, comparing experimental and numerical test. They found a correlation between experimental and numerical data. Gonzalez-Gutierrez et al. [17] studied the dimensional stability and shrinkage on chromium-rich tool steel powder when varying the powder content from 50 to 60 vol%. It was observed that the highest powder content leads to more constant dimensions during extrusion, with a more linear shrinkage along three dimensions. Huang and Hsu [18] elucidated the effects of key injection molding and sintering parameters on dimensions and mechanical properties of 316L stainless steel MIM parts. As previously observed, the sintering temperature is crucial to determine the dimensional shrinkage rate, density, but also the hardness of the sintered parts. Kurose et al. [19] reported how the shrinkage evaluated on 316L MEX parts was closely dependent on the printing orientation and they proposed a theory to explain the anisotropic shrinkage mechanism. According to [20], this behavior may be attributable to the internal stresses generated within the printed parts. Gonzalez-Gutierrez et al. [21] analyzed copper samples with a rectangular cross-section and they found a considerable shrinkage along the filament deposition direction, leading to an anisotropic shrinkage. Ait-Mansour et al. [22] analyzed the shrinkage behavior on tensile samples and on compression pins realized by using MEX and a commercial 316L filament, by varying respectively, the printing orientation and the theoretical infill levels. Caminero et al. [23] assed the effects of printing parameters on dimensional accuracy of 316L stainless steel samples realized by MEX, using predictive models based on artificial neural networks and they also conducted an analysis of the mechanical and microstructural characteristics. Jiang and Ning [24] compared the numerical, analytical and experimental results on overhang structures realized by Metal MEX using a commercial 316L feedstock material. They observed how the gravity force affected parts with high overhang angle.

It is worth highlighting that few studies are exclusively focused on the evaluation and comprehension of the shrinkage phenomenon. In most cases, dog-bone samples, characterized by standardized dimensions and fillets, were used as test samples, since the main goal of those studies was related to the mechanical behavior evaluation. Moreover, the reported studies did not investigate the effect of

the shrinkage on the geometric accuracy. For understanding the considered phenomenon and its implications on the geometric accuracy of the manufactured parts, 3D scanning methods are preferable due to their completeness of information [25].

In this paper, a comprehensive study about the shrinkage phenomenon was conducted using a commercial 17-4 PH metal-composite filament. Shrinkage percentage values were evaluated along the main axes and geometric accuracy was also assessed by using a 3D structured-light scanner, which enabled a deep analysis on both green and sintered parts. It is worth mentioning that, to the authors knowledge, the shrinkage behavior of the used feedstock is not yet documented in literature, neither the geometric accuracy of the sintered parts, quantitatively. Density was also evaluated on both as-printed and as-sintered parts. Using the Design of Experiment (DoE) approach, 24 samples were printed varying printing and sintering orientation, infill strategy and aspect ratio. More in details, the printing/sintering orientation effect on the shrinkage behavior was assessed by considering two main conditions: the printing orientation coincident with the sintering orientation (P=S), and the printing orientation different from the sintering orientation (P≠S). The material supplier guidelines suggest printing and sintering using the same object orientation during printing and sintering. However, this recommendation is sometime impractical for several reasons, e.g. the furnaces limited dimensions that constrain the orientation of the sample during sintering, as well as the sintering of samples characterized by high aspect ratio which could collapse during sintering if not properly oriented. In these cases, the printing orientation may be different from the sintering orientation. Aspect ratio and infill line strategies were also investigated, as their effect on shrinkage and geometric accuracy was not sufficiently studied in literature.

2. Material and Methods

For the conducted experiments, a set of samples was fabricated using the commercial BASF Ultrafuse® 17-4 PH filament (BASF 3D Printing Solutions GmbH, Germany) composed by a high-weight percentage (≃88%) of 17-4 PH powder and a mixture of polyoxymethylene (POM) and polypropylene (PP). POM is used for the catalytic debinding which decomposes into smaller molecules in presence of a catalyst when exposed to the appropriate temperature (approximatively 120 °C in nitric acid or oxalic acid), while PP ensures a sufficient stability of the part during sintering [26]. This phase occurs in dry hydrogen atmosphere with a pre-heating at 5 °C/min, from room temperature to 600 °C for 1h of holding time and a subsequent heating at 5 °C/min, from 600 °C to 1300 °C and 3h of holding time. The D&S phases were performed outside at the ELNIK Systems GmbH (Waldachtal, Germany).

Ultimaker Cura® was used as slicer and the samples were printed on Creatbot F430 (Henan Creatbot Technology Limited, China) using a nozzle with a ruby tip and a diameter of 0.6 mm. To avoid warpage on the part, the glue stick Magigoo® Pro Metal was used for each sample.

All samples were realized by using these main 3D printing parameters, previously optimized, and kept constant during the conducted experiments: layer height = 0.15 mm, wall lines number = 2, printing speed = 30 mm/s, infill density = 100%, infill overlap = 10%, flow rate = 120%, nozzle temperature = 260 °C and bed temperature = 100 °C.

The shrinkage effect was then investigated by using a 2^3 factorial design and the test samples were randomized. Three factors were considered, printing/sintering (P/S) orientation, infill line strategy, length/width aspect ratio and two levels for each: printing=sintering (P=S) or printing≠sintering (P≠S), 0° or 90° for the infill line strategy and, finally, the aspect ratio 1:1 or 5:1 (see **Table 1**).
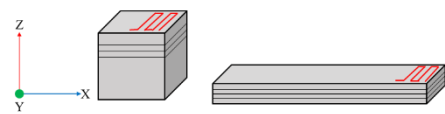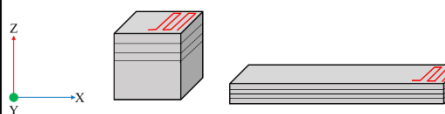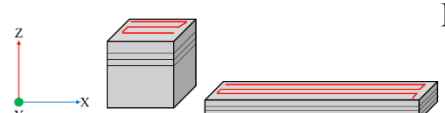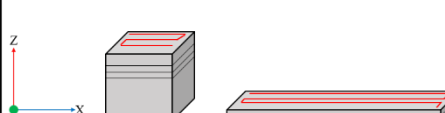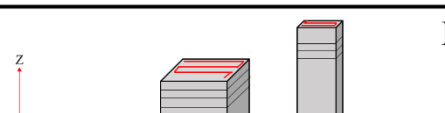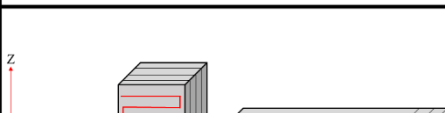
By analyzing the condition (P≠S), it was possible to separate the shrinkage amount along printing and sintering directions, providing useful information for end users and companies which are interested in producing complex geometries with printing and sintering orientation not coincident.

The printing direction is defined as the growing direction during printing (orthogonal to the layer plane), while the sintering direction is defined as the direction along which the gravity force acts during the sintering. The infill line strategy is referred to the direction of filament deposition or raster direction. Varying the aspect ratio two kinds of geometries were obtained: a cubic sample with 15 mm of edge length and a parallelepiped sample (bending-like) with a rectangular cross-section (length = 80 mm, width = 15 mm, thickness = 6 mm). Three replicas for each condition were realized.

Table 1 Factorial design parameters. In parenthesis the abbreviations for the nomenclature of samples group.

P/S orientation	Infill line strategy	Aspect ratio
Printing=Sintering (P=S)	0° (0)	1:1 (1)
Printing≠Sintering (P≠S)	90° (90)	5:1 (5)

A graphical summary of the different samples investigated is reported in **Fig. 1**. The red lines are referred to the infill line strategy (raster), while the black ones to the layers. For each group of samples involved, the orientation during printing and during sintering are also shown, for sake of clarity.

Fig. 1. Configurations studied in the work.

After D&S phases, the polymeric fraction is removed from the part and the dimensions become smaller. In order to achieve the desired dimensions, the oversizing of the green parts is required. This latter was applied complying with the material supplier guidelines. Thus, an oversizing of 126% was applied along the sintering direction, the Z axis on the "Sintering" column of **Fig. 1** (where a shrinkage of 20% is expected), while for the other dimensions, X and Y axes, the oversizing was set to 119% (where a shrinkage of 16% is expected).

The fabricated samples were then reconstructed and measured in their as-printed (green) and as-sintered (sintered) conditions by using a commercial 3D structured light scanner, ATOS Q 8M supplied by ZEISS GOM Metrology (Zeiss Corp., Germany), with a working area of 100 x 70 mm^2 and a declared resolution of 0.04 mm (from manufacturer specification).

The density of green and sintered samples was measured applying the Archimedes' Principle [27] with a dedicated equipment. With this method, only cubic samples were tested due to equipment size limits. Moreover, another method for the density evaluation was considered: the weight/volume ratio obtained by using a precision balance (d = 0.001 g) for the weight evaluation and the volume computed by the GOM Inspect software on the obtained 3D models. The subsequent dimensional analyses were conducted using the GOM Inspect software and the same measurement procedure was applied on the as-printed and as-sintered samples. More in details, each dimension (length, width and

height) was assessed as distance between corresponding points lying on two opposite faces of the sample. The average value was computed considering approximately 20 points for each dimension. The shrinkage was evaluated at first considering the X, Y and Z axis directions (**Fig. 1**). However, since those directions can have different meaning when the printing orientation is different from the sintering orientation, other more meaningful directions were considered: sintering (S) direction, printing (P) direction, infill line (INF) and orthogonal infill line (O-INF) direction, see **Fig. 2**.
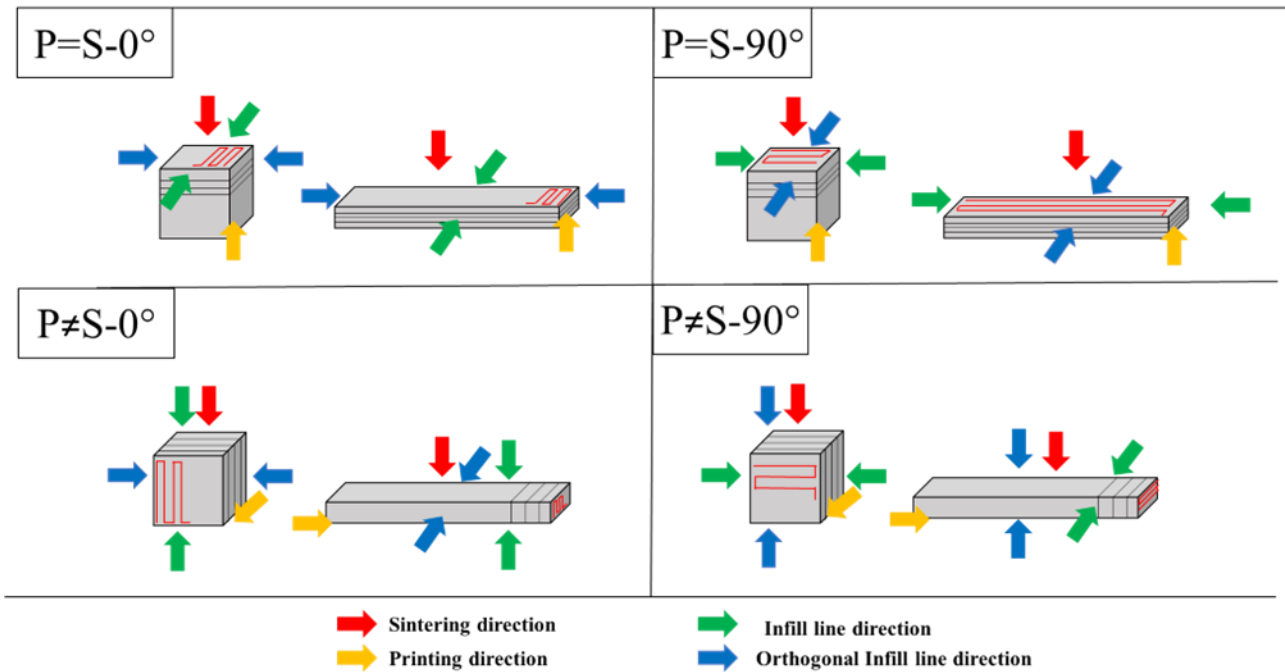
Fig. 2 Main directions considered for the shrinkage evaluation and for each configuration involved.

The geometric accuracy was also investigated on both green and sintered parts. With this purpose, being the samples cubes and parallelepipeds, the flatness was assessed on each face and the effect of sintering was evaluated by considering the same directions reported in **Fig. 2**. The flatness was computed each time as the average value of a couple of faces, e.g., top and bottom, left side and right side, front and back, with the aim to evaluate the amount of geometric error along printing, sintering and infill line direction. More in details, the considered faces were the ones orthogonal to the specified direction. The labels "top and bottom, left side and right side, front and back" refer to the position of the surfaces during the sintering phase. As an example, for the configurations where P=S, the flatness evaluated on the top and bottom faces corresponded to the printing/sintering direction, as it coincides with their normal direction. Surface comparisons were also carried out between each face and an ideal plane to better analyze the occurrence of geometric distortion related to each considered direction.

3. Results and Discussion

## 3.1 Density evaluation on as-printed and as-sintered samples

The densities of as-printed and as-sintered samples measured through the Archimede's principle and using the weight/volume ratio method, are reported in **Table 2** as the average value ± standard deviation evaluated for each group of samples.

Table 2 Values of green density derived from Archimede's test.

| Group of samples	Green Archimede density (g/cm^3)	Green density (g/cm^3) ratio method	Sintered Archimede density (g/cm^3)	Sintered density (g/cm^3) ratio method
P=S-0-1	4.22±0.06	4.24±0.05	6.84±0.09	6.89±0.09
P=S -90-1	4.20±0.03	4.23±0.03	6.77±0.08	6.82±0.08
P≠S-0-1	4.20±0.12	4.23±0.09	6.77±0.25	6.80±0.25
P≠S -90-1	4.24±0.13	4.24±0.11	6.94±0.27	6.90±0.28
P=S -0-5		4.31±0.02		7.06±0.04
P=S -90-5		4.27±0.02		6.82±0.09
P≠S -0-5		4.35±0.01		7.10±0.02
P≠S -90-5		4.47±0.01		7.32±0.01

From the experimental results, there was a good agreement between densities evaluated among the investigated groups of samples. In particular, the green cubic samples showed more homogeneous density values comprised in a range between 4.20 and 4.24 g/cm^3. The green bending samples, instead, reported a slight variability and the density values were comprised in a range between 4.27-4.47 g/cm^3. Considering the as-sintered samples, the average values for the cubic samples were lower than 7.00 g/cm^3, and a higher standard deviation was found for the P≠S samples. As already mentioned in Material and Methods section, the density of the parallelepipeds was evaluated as the ratio between the measured weight (g) and volume (mm^3). This latter was computed by the GOM Inspect software, using the 3D reconstruction of the sample (see **Table 2**). A good correspondence between the implemented methods was found for the cubic samples, with approximately 0.2%-0.6% of difference between the ratio method and the Archimedean one. The lowest value of sintered density was recorded for P≠S-0-1 and P=S-90-1 (6.77 g/cm^3 according to Archimedes' test) due to the delamination between infill lines and the wall lines for the first group, as reported in **Fig. 3**a. This defect was observed also on the parallelepipeds samples P=S-90 and in other previous works [13,21,28]. This group, in fact, reported the lowest values of sintered density (6.82±0.09 g/cm^3) among the parallelepipeds samples. Typically, these defects, already observed on the green parts, to a lesser extent, are amplified after the D&S process, due to the binder removal and the shrinkage phenomenon. Moreover, the D&S can induce some other defects, such as porosity, warping, balling

and distortion [20,29]. The main effect is a reduction of density, as confirmed in this work, and consequently of the mechanical performance. In **Fig. 3a-b**, the defects reported on sintered parts.
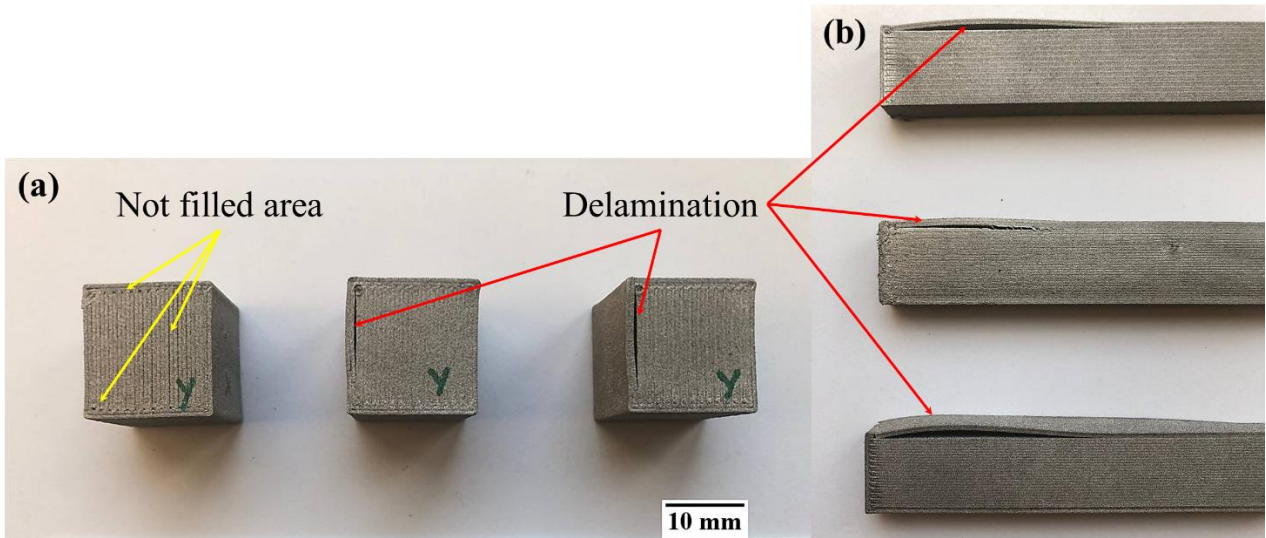
Fig. 3. Defects on 17-4 PH samples after sintering: a) P≠S-0-1 and b) P=S-90-5.

Before the shrinkage evaluation, a first check was made considering the volume of each sample and its deviation with respect to the nominal CAD value (evaluated on both, green and sintered parts). Results are reported in **Fig. 4**. All samples showed a negative volume deviation comprised between -0.04% and -2.75% for the cubic green parts, while a mostly positive volume deviation was registered for parallelepipeds. All the investigated groups reported a lower value of sintered volume with deviations comprised between -4.95% and -8.21% when compared to the nominal one, highlighting that the oversizing factors used did not allow to obtain accurate dimensions.
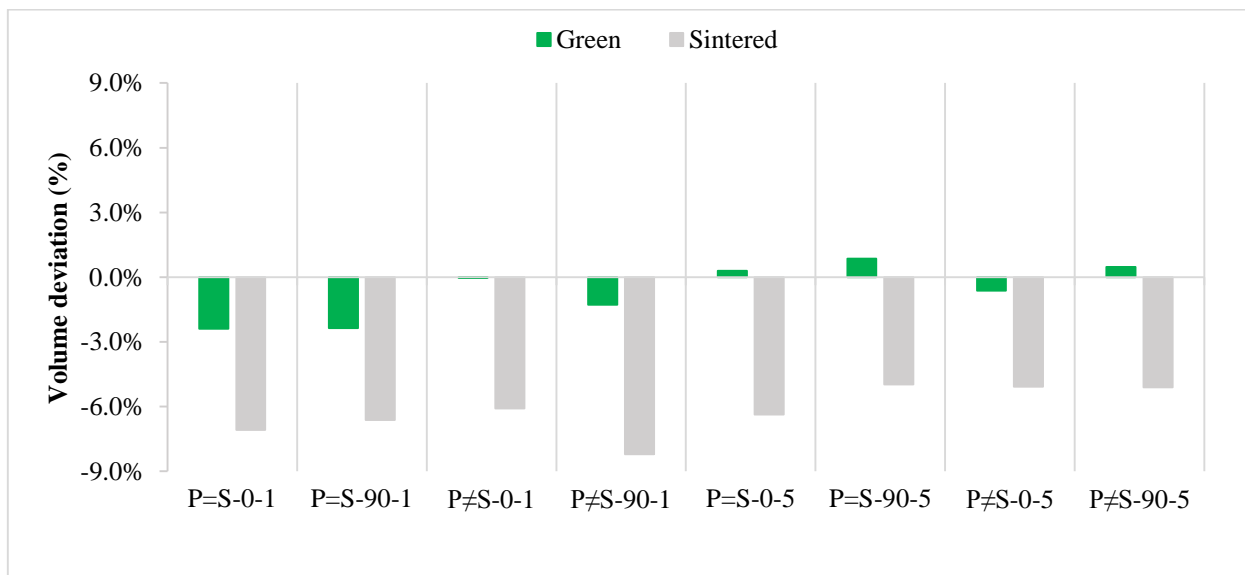

Fig. 4. Volume percentage deviation of green and sintered for the investigated groups.

9

3.2   Shrinkage evaluation

The shrinkage phenomenon is the reduction of the volume and weight affecting the green part after the debinding and sintering. It is usually computed using the **Eq.1** for each involved dimension (length, width and height).

$$\text{Shrinkage (\%)} = \left(1 - \frac{\text{Sintered dimension}}{\text{Green dimension}}\right) * 100 \tag{1}$$

The shrinkage results are shown in **Fig. 5**. More particularly two graphs are reported. The first (**Fig. 5a**) is dedicated to samples printed and sintered with the same orientation (P=S), while the second (**Fig. 5b**) is dedicated to the other condition, where the printing orientation was different from the sintered one (P≠S). The shrinkage was grouped for the three main axes X, Y and Z (see **Fig. 1**, "sintering" column).
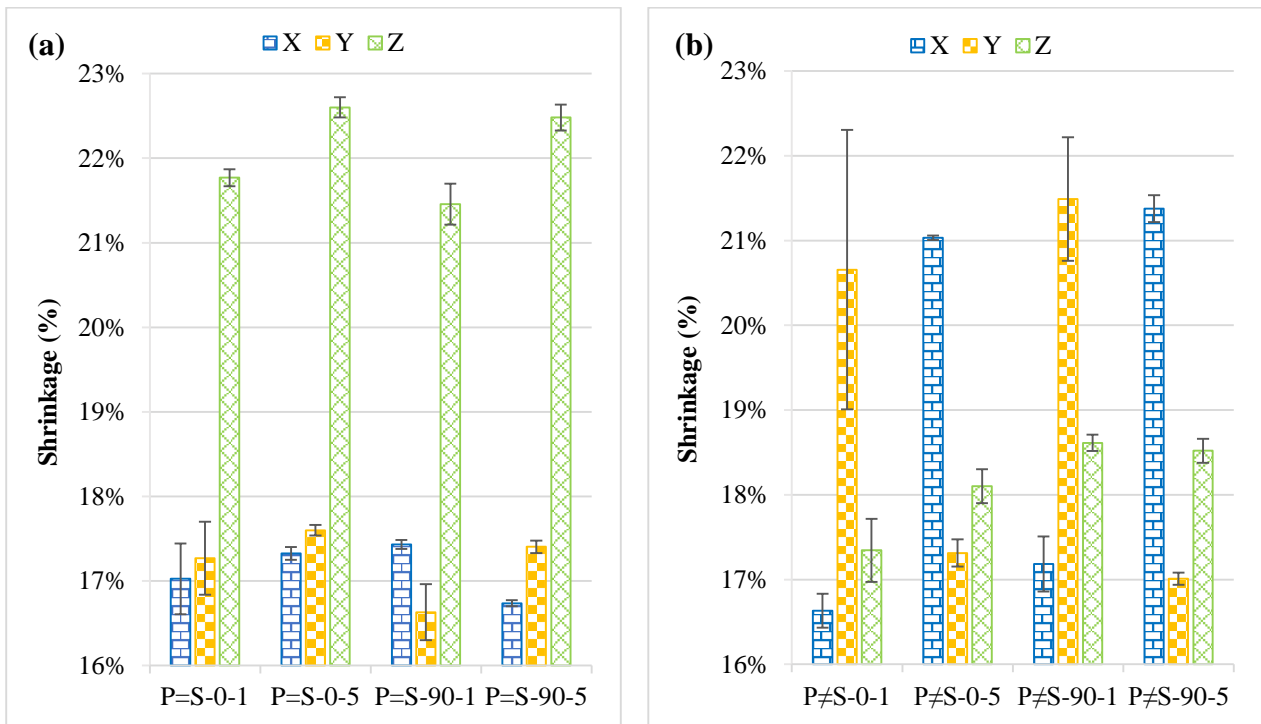
Fig. 5. Average values of shrinkage for (a) Printing = Sintering configuration and (b) Printing ≠ Sintering configuration.

Considering the first configuration (P=S), the Z axis coincided with both printing and sintering directions, while X and Y were parallel or orthogonal to the infill line direction (**Fig. 6**). As expected, the samples with the same printing and sintering direction (**Fig. 5a**) reported the highest shrinkage along the Z-axis, the printing/sintering direction, in a range comprised between 21.5% and 22.6%. In this configuration, the effects of both, printing and sintering directions, on the shrinkage evaluated on Z, added to each other. As reported in previous works, one of the factors that influence the amount of shrinkage, during the sintering process, could be the gravity force, that squeeze the layers among

10

them, filling voids created during the printing phase [13,19,20,29]. The X and Y axes instead, reported slight differences of shrinkage due to the unidirectionality of the infill line strategy.
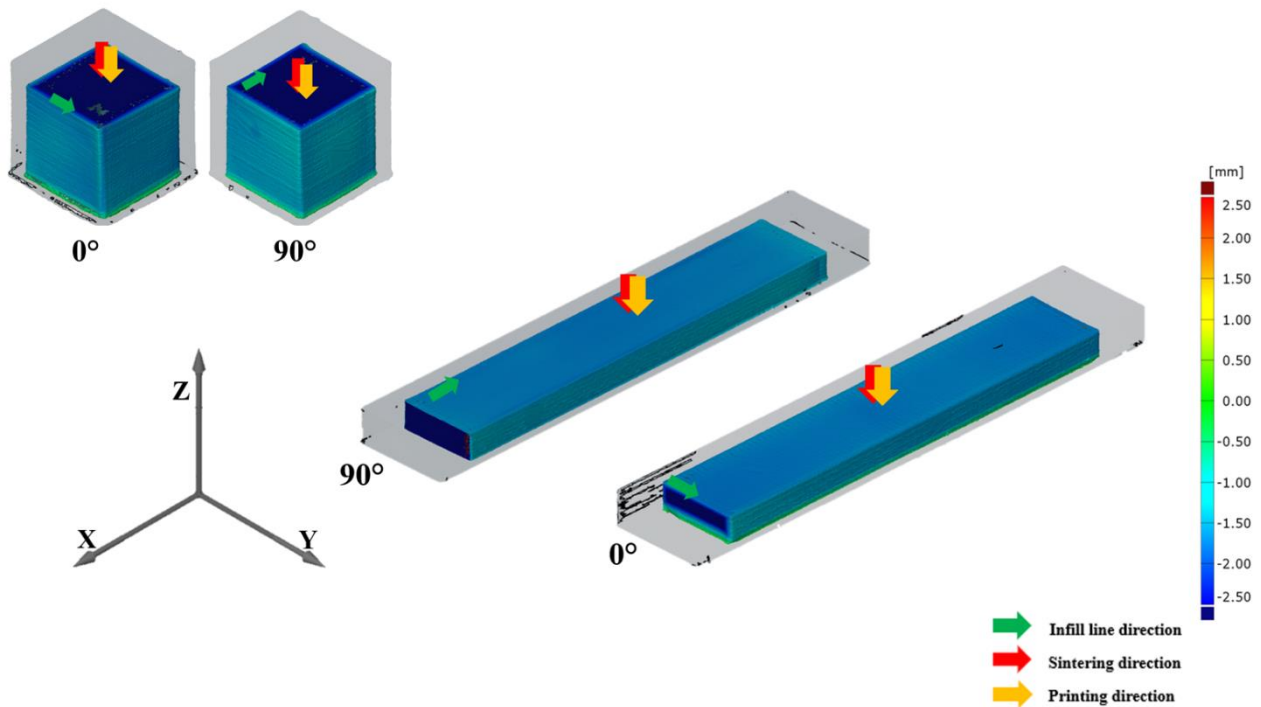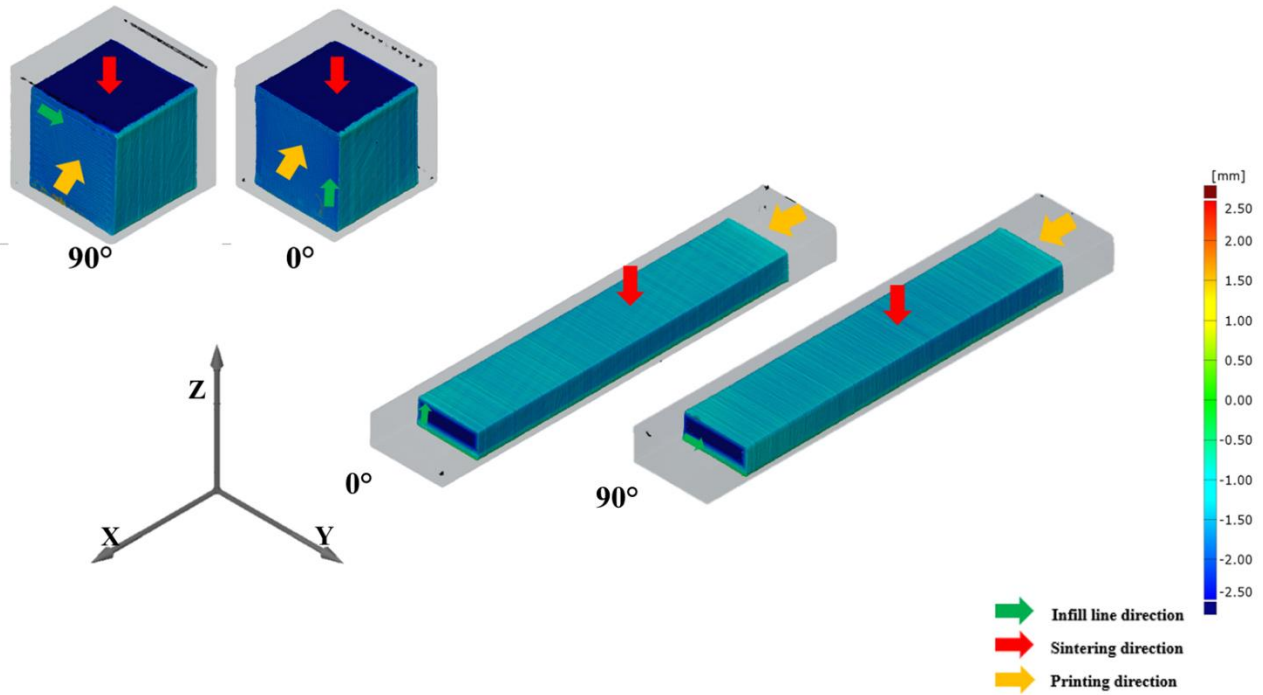

Fig. 6. 3D comparisons between green and sintered parts with the main directions highlighted (configuration P=S).

More complex was the interpretation of data reported in **Fig. 5b**, showing the case where the printing orientation is different from sintering. In this condition, indeed, the shrinkage evaluated on X, Y and Z axes has a different meaning for each sample, see **Fig. 2**. More in details, the Z axis still represents the sintering direction, but it does not anymore represent the printing direction.

As reported in **Fig. 7**, the samples were placed during the sintering in the XY plan, so the Z axis of printing direction was not coincident to the Z axis of sintering (see **Fig. 1**-"Sintering" column).

In this case, the sintering direction (Z axis) was not the one characterized by the highest shrinkage, since the highest values (above 20%) were observed along the printing direction.

Fig. 7. 3D comparisons between green and sintered parts with the main directions highlighted (configuration P≠S).

In order to provide an easier understanding of the obtained data, rather than considering the shrinkage on the X, Y and Z axes, it was evaluated on respectively, the printing, sintering, infill line direction and orthogonal to the infill line direction. This means that, considering the first configuration, P=S, the main directions would be printing/sintering (P/S), infill line direction (INF), orthogonal to the infill line direction (O-INF).

While, considering the printing not coincident with sintering, the main directions would be: sintering (S) and printing (P), infill line direction (INF) and orthogonal to the infill line direction (O-INF). In some cases the sintering direction can be coincident with the INF (when the infill strategy is 0° oriented) or the O-INF direction (when the infill strategy is 90° oriented). Data were then reorganized accordingly, and they were represented by interval plots. In the following subsections, the effect of each factor involved in the factorial design was better analyzed.

3.2.1   Printing and Sintering orientation

In **Fig. 8** interval plots of the P=S and P≠S are reported. This representation allows to confirm that when printing and sintering direction were the same, the shrinkage was higher along the printing/sintering direction (**Fig. 8a**). In the condition P≠S, the direction with maximum shrinkage was the printing direction, followed by the sintering direction, while the other directions connected to the filament orientation showed lower shrinkage values (**Fig. 8b**).
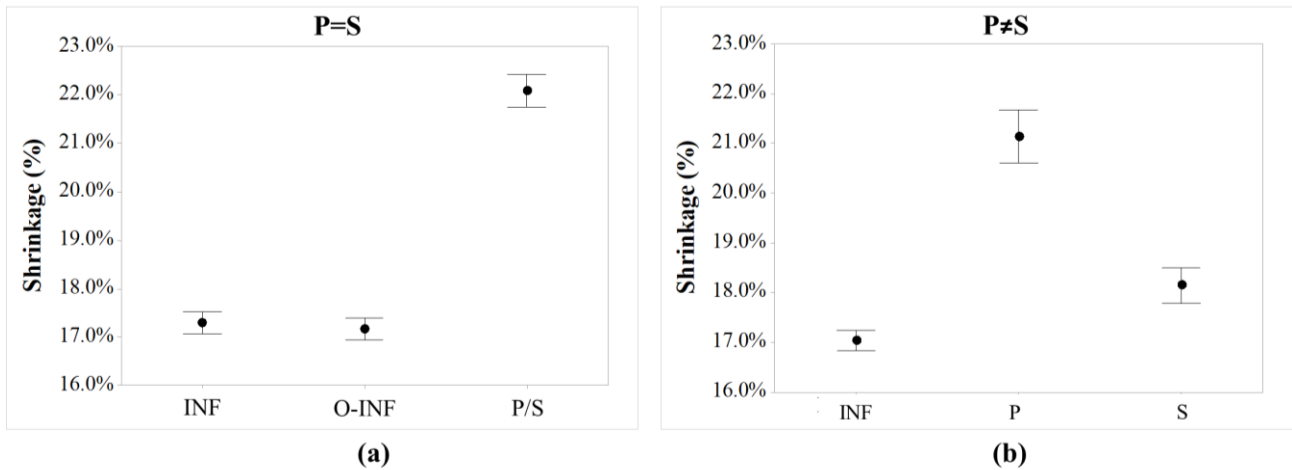
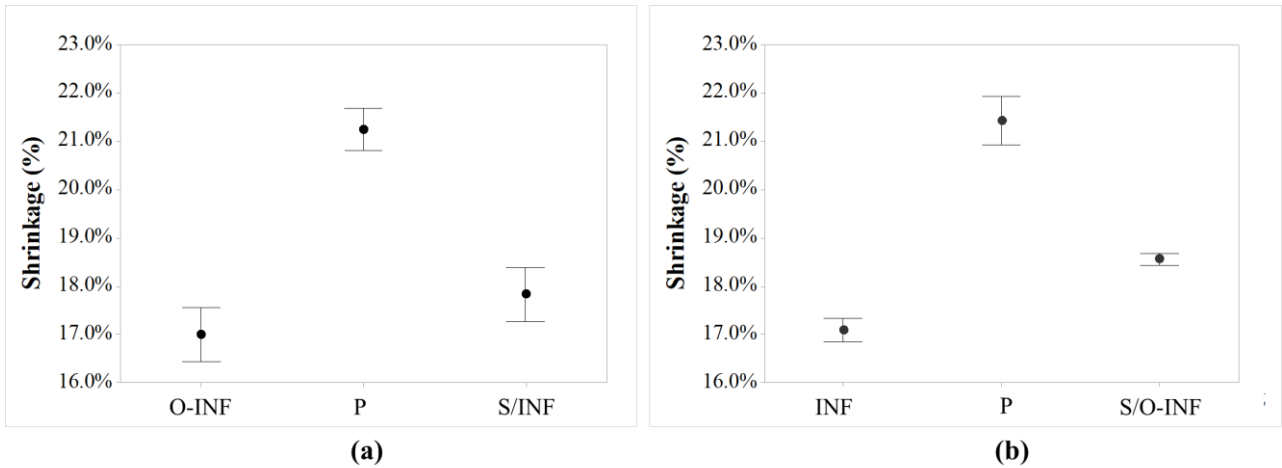**Fig. 8.** Interval plot for shrinkage (a) P=S (b) P≠S

The shrinkage along the printing/sintering (P/S) direction and the shrinkage along the printing (P) or sintering (S) directions, were further analyzed with Pareto chart of standardized effect. The considered factors were then the infill line strategy and the aspect ratio. In **Fig. 9a**, the Pareto chart of the shrinkage along printing direction for P≠S is reported. As it is possible to observe, none of the factors affected the shrinkage along the printing direction (**Fig. 9a**), meaning that, regardless of the factor considered, the dimension along the printing direction shrunk more than the other directions. While, the shrinkage evaluated along the sintering direction (**Fig. 9b**) showed how all the considered factors were significant, in particular the infill line strategy was the most relevant. Instead, in **Fig. 9c** was reported the Pareto chart for shrinkage along the P/S direction (P=S configuration). It was found that the aspect ratio was the most influencing factor. This result confirmed the values reported in **Fig. 5a** for P=S-0-5 and P=S-90-5.

13
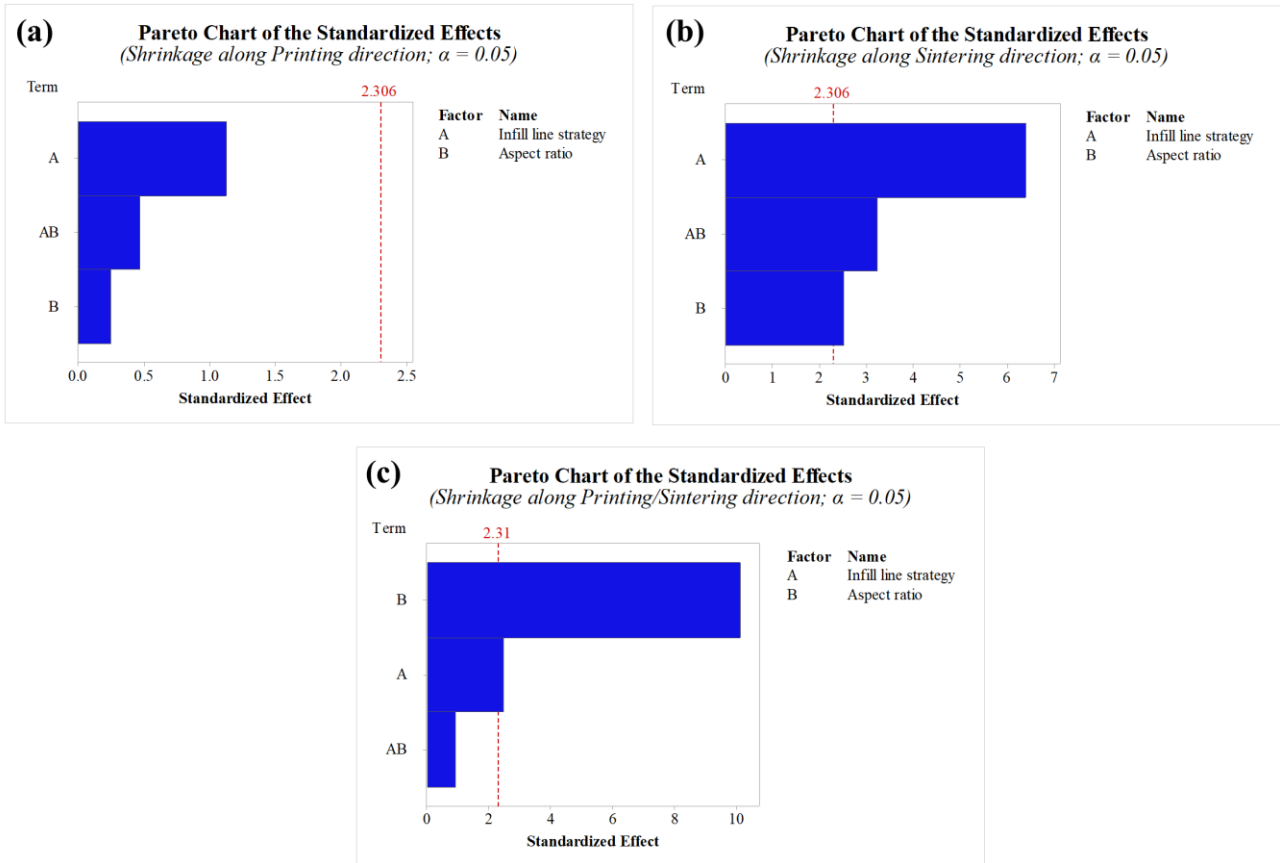
Fig. 9. Pareto charts: (a) shrinkage along the P direction in P≠S configuration (b) shrinkage along the S direction in P≠S configuration and (c) shrinkage along the P/S direction in the P=S configuration.

3.2.2 Infill line strategy

The configuration with printing and sintering differently oriented is further analyzable, by varying the infill line strategy. In one case (orientation at 0°), the infill line direction is coincident with the sintering direction and in the other case (orientation at 90°) it is the opposite (see **Fig. 2** and **Fig. 7**). This factor was indeed found significant according to the one-way ANOVA, considering as output the shrinkage along the sintering direction (p-value=0.002) and according to the Pareto chart reported in **Fig. 9b**. It emerged that when the direction of sintering was orthogonal to the infill line direction (**Fig. 10b**), the shrinkage was higher (18.4%-18.7%) while, when the sintering direction was coincident with the infill line direction the shrinkage was lower (17.3%-18.4%), as reported in **Fig. 10a**.
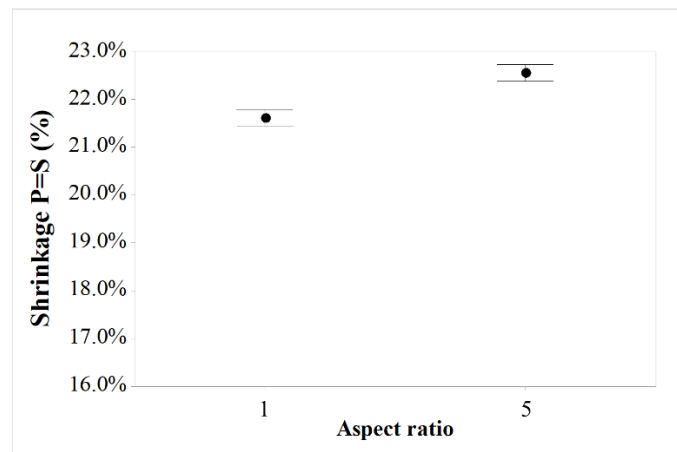
Fig. 10. Interval plot for the shrinkage for cubic and bending samples with (a) P≠S-0 and (b) P≠S-90.

On the other hand, no significant differences were registered between the shrinkage along the INF direction and the O-INF in the condition P=S, where the two groups of samples registered overlapping values of shrinkage (see **Fig. 8a**).

3.2.3 Aspect ratio

Considering the aspect ratio, in the configuration P=S, the one-way ANOVA showed that it was influent when considering the shrinkage along the P/S direction (p-value$<<0.05$), as reported in **Fig. 11**. Shrinkage values were comprised within 21.4% and 21.8% for cubic samples, while they were higher for the bending ones, reaching values comprised between 22% and 23%. These results reinforced the results of the Pareto chart reported in **Fig. 9c**, where the aspect ratio was the most relevant factor for the shrinkage along the P/S direction.

Fig. 11. Interval plot of the shrinkage P=S for cube and bending samples

This difference could be related to a lower thickness of bending samples compared to the cubic samples. This behavior could confirm what was reported by Galati and Minetola [30] on 17-4 PH

15

parts, where a different amount of shrinkage was related to the different dimensions and filling strategy. The same factor was found instead not relevant for the configuration P≠S (p value >>0.05).

3.2.4   Summary of shrinkage results

To summarize, when P=S, the shrinkage was on the order of 16.6%-17.5% on X and Y axes, while along the printing/sintering direction (Z axis) it was higher and approximately equal to 21.5% for cubic sample and higher than 22% for the parallelepipeds sample. In the configuration P≠S, the shrinkage was comprised between 17.3% and 18.6% along the sintering direction, between 20.7%-21.5% along the printing direction and about 17% along the remaining direction (infill line direction or the orthogonal one). The maximum value of shrinkage was achieved in the P=S condition and with 5:1 aspect ratio (close to 23%). In this case, indeed the effect of the sintering and printing directions added to each other. When P≠S, the maximum shrinkage was slightly lower since, in this case, those two directions are not coincident.

It is worth highlighting that in this work it was possible to evaluate the specific influence of the sintering direction and of the printing one, separately, when the configuration P≠S was considered. This is of great importance, since very often it is required to print a sample with a specific orientation and to sinter it using another orientation (e.g., high aspect ratio, furnace maximum dimensions) and in this case the oversizing factors must be properly chosen.

From the conducted analyses, a correlation between the volumetric shrinkage and the sintered density was also assessed. After sintering, the samples shrunk of about of 46.4% in volume and an overall average weight loss of 12.6% was also recorded. The highest shrinkage in volume (47.0%) was observed for the P≠S-90-1 group. This higher volumetric shrinkage caused an increase in the sintered density, as observed by Singh et al [15]. **Fig. 12** showed the correlation between the volumetric shrinkage and the increase of density from the green to the sintered condition. The first term, was evaluated considering the volumes received from GOM Inspect software, instead the second term was related to the densities reported in **Table 2**.
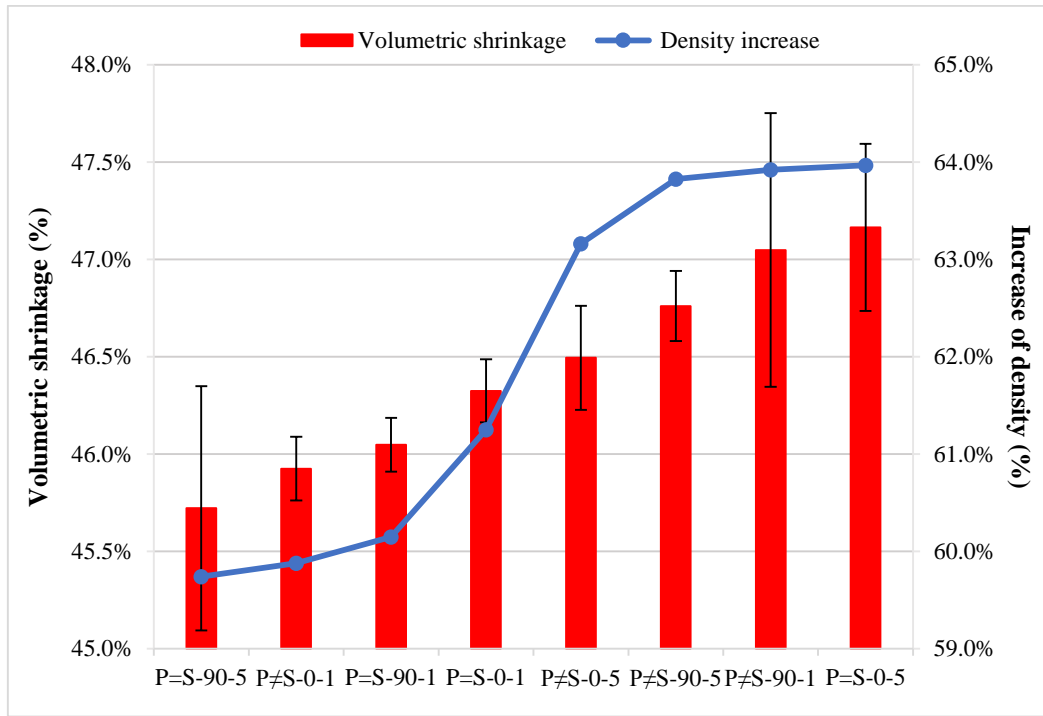
Fig. 12. Correlation between shrinkage volume (%) and increase of density (%).

3.3 Geometric evaluation

Another aspect investigated in this work was the effect of the printing and sintering orientation on the geometric accuracy of the obtained samples. With this aim, the flatness was computed on each sample face, according to the methodology reported in the Material and Methods section. Thus, each group of samples was analyzed and the flatness evaluated on each couple of planes orthogonal to the considered direction (sintering, printing, infill line and orthogonal infill line).
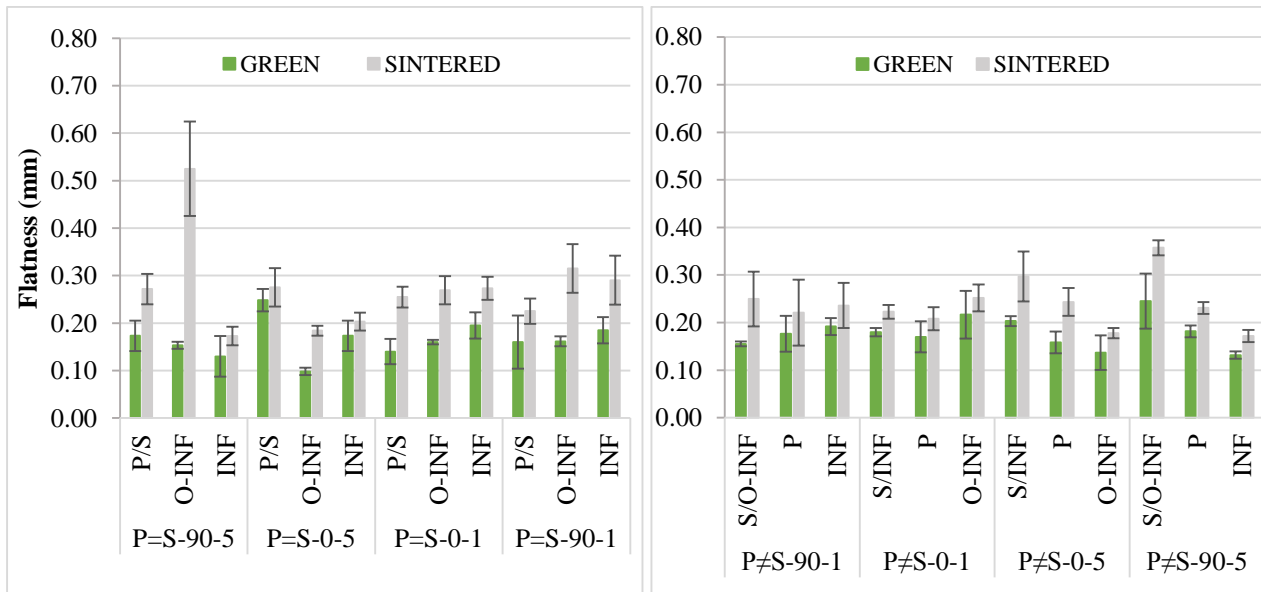

Fig. *13*. Flatness evaluated for each group of samples along sintering, printing and infill line directions.

As it is possible to observe from **Fig. 13**, flatness values were generally below 0.2 mm for the green parts, while they were comprised between 0.25 mm and 0.35 mm for the sintered parts, denoting a worsening effect of the sintering on the geometric accuracy. When considering the P=S configuration, the maximum value of flatness was achieved for the group of samples P=S-90-5 along the O-INF direction (>0.5 mm) where delamination occurred (see **Fig. 3b)** and along the same direction for the group of samples P=S-90-1 (>0.3 mm)**.** For what concerns the P≠S configuration, the highest values of flatness were registered along the sintering direction for parallelepipeds (P≠S-0-5 and P≠S-90-5), while quite homogeneous values were registered when considering cubic samples (P≠S-0-1 and P≠S-90-1). Although, for the samples P≠S-0-1 delamination occurred along the O-INF direction (see **Fig. 3a)** and the geometric error was prevalent along this direction. The maximum value of flatness was achieved along the sintering direction for the group of samples P≠S-90-5. In this case the sintering direction coincided with the O-INF and a high shrinkage was also achieved. The effect of sintering on the geometric error was also investigated considering a surface comparison between each sample face and a corresponding ideal planar surface. These comparisons allowed to evaluate the amount of geometric distortion along the main identified directions. Colored maps and histograms are reported in **Fig. 14** and **Fig. 15**. Histograms refer only to the deviations evaluated on the sintered part.

For what concerns the P=S configuration (**Fig. 14Error! Reference source not found.**), surface distortions were detected for both cubes and parallelepipeds mostly in the as-sintered condition. The top/bottom surfaces registered high deviations in most of the analyzed cases and this effect could be attributable to the printing/sintering combination and to the effect of the gravity force (more marked at the center of the sample top surface). Along that direction the maximum shrinkage was also achieved. Significant deviations were also registered along the INF and O-INF directions for what concerns the cubes, while considering the parallelepipeds and, in particular the group of samples P=S-90-5, the geometric distortions were prevalent along the O-INF, if compared to the INF direction, where delamination was observed (see **Fig. 3b**).
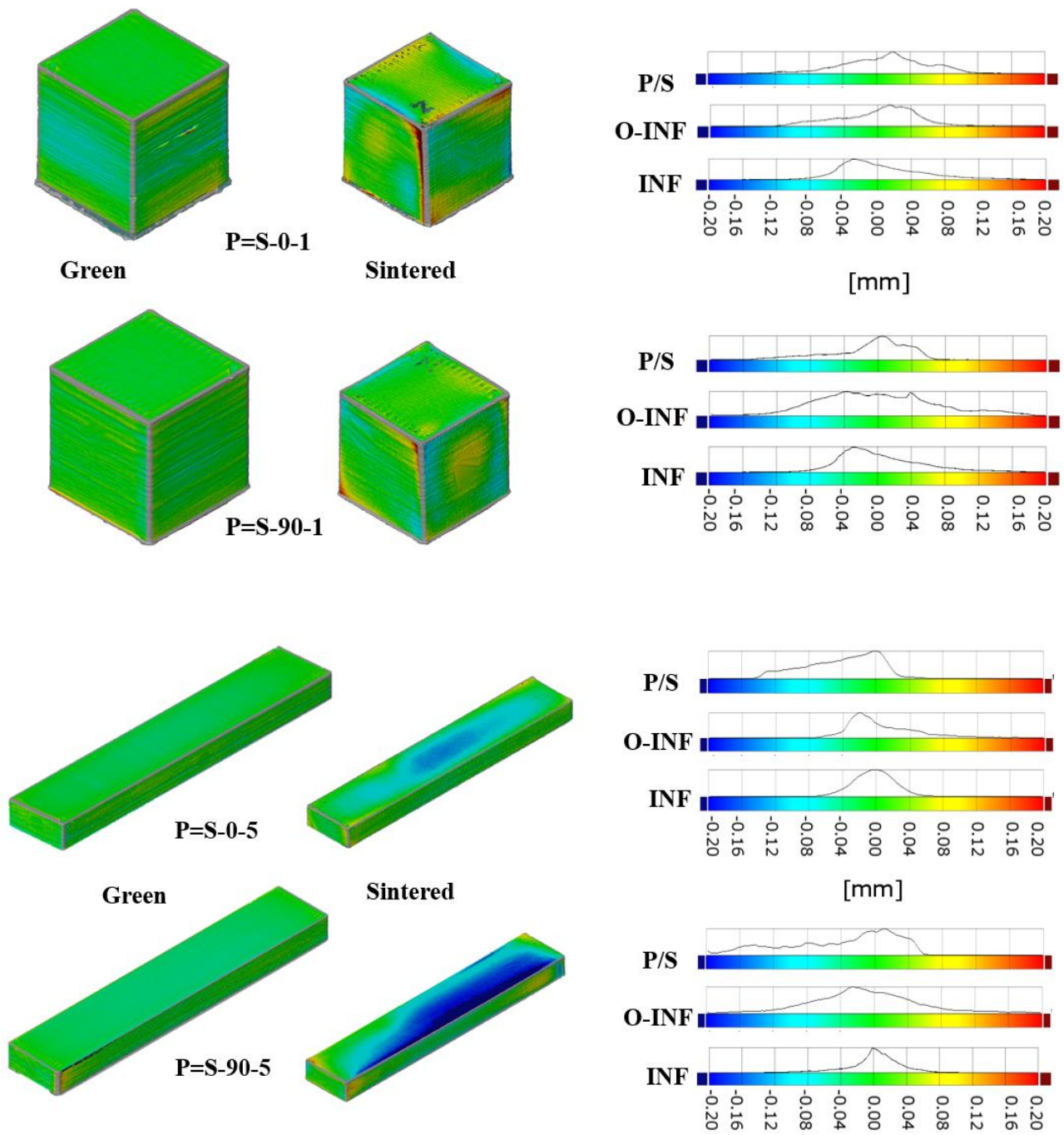
Fig. 14. Colored maps and histograms showing the deviation of each pair of surfaces with respect to ideal planes (P=S).
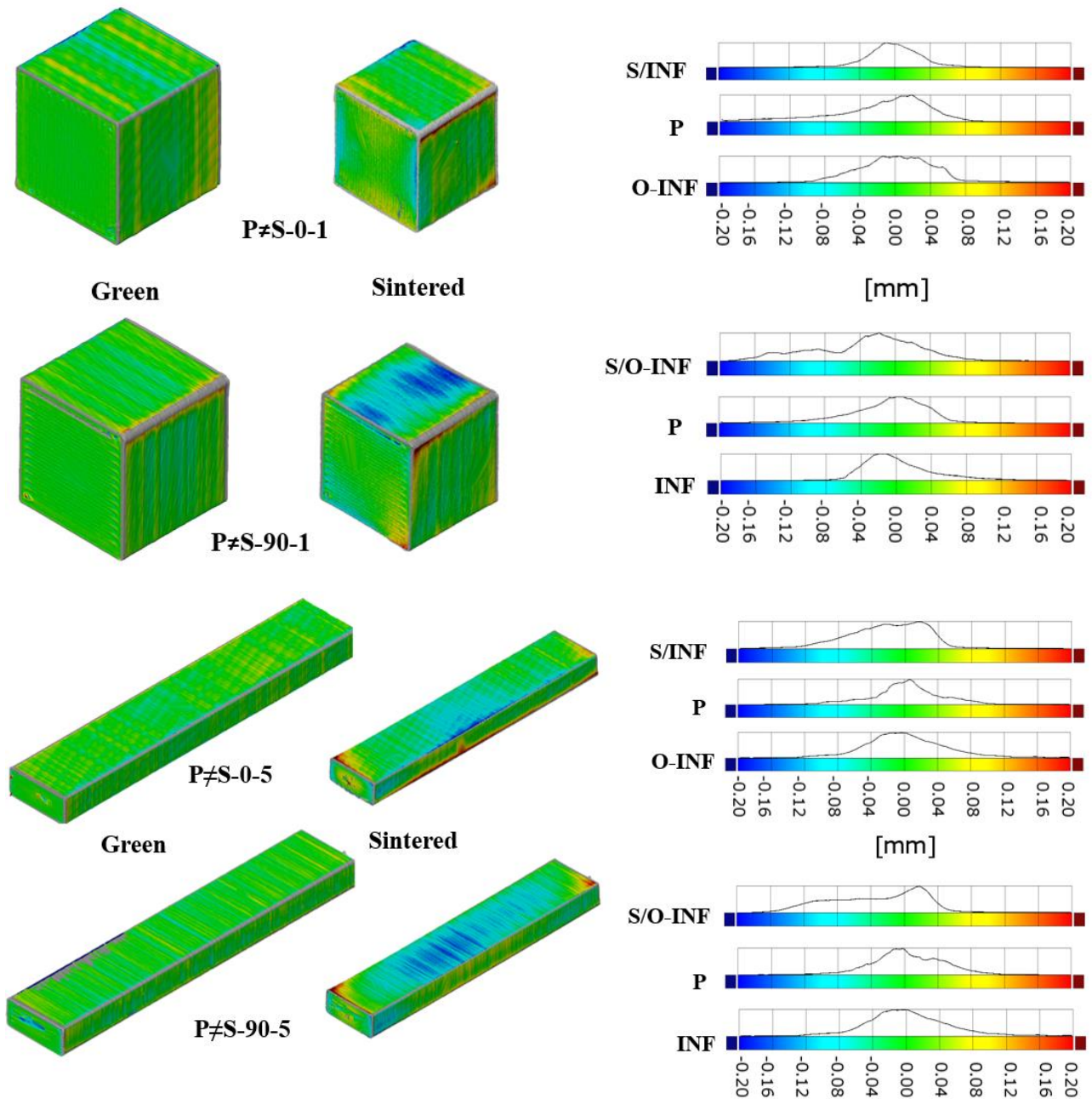
Fig. 15. Colored maps and histograms showing the deviation of each pair of surfaces with respect to ideal planes (P≠S).

When P≠S (see **Fig. 15**), the geometric deviations were mostly observed along the sintering direction and in particular where this direction coincided with the direction orthogonal to the infill line (S/O-INF direction). A slightly different behavior was observed for the group of samples P≠S-0-1, where delamination occurred along the O-INF direction (see **Fig. 3a**).

In some cases, a relation between the shrinkage and the geometric distortion was detected. To better understand this aspect, the shrinkage values were compared with the flatness variation evaluated between the sintered and the green parts (Δflatness). Flatness variations were always positive, meaning that the flatness on sintered samples was always higher than the flatness evaluated on the

green samples. This way, the flatness variation can be used to quantify the worsening effect of the sintering on the geometric accuracy. Results are shown in **Fig. 16** and **Fig. 17**. For the configuration P=S, three main clusters could be recognized, and they were differentiated either by the shrinkage alone (e.g., shrinkage along P/S direction), or by the flatness alone (e.g., delaminated samples), meaning that no correlation was found between shrinkage and flatness variation. For what concerns the configuration P≠S, similar considerations can be drawn, except for the cluster marked with a yellow circle in **Fig. 17,** where to a higher shrinkage corresponded a higher value of flatness variation, showing a worsening of the geometric accuracy (see also **Fig. 15**).
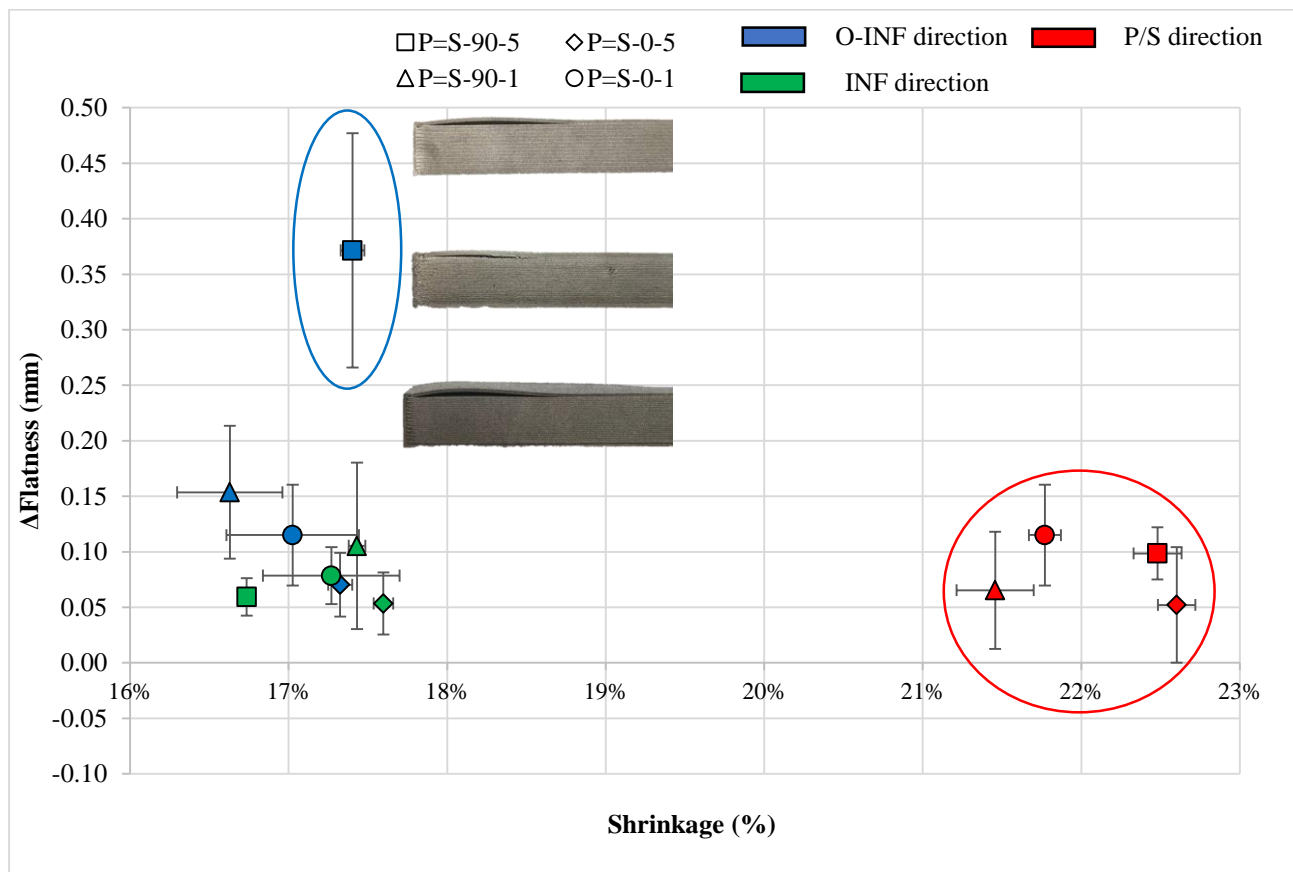
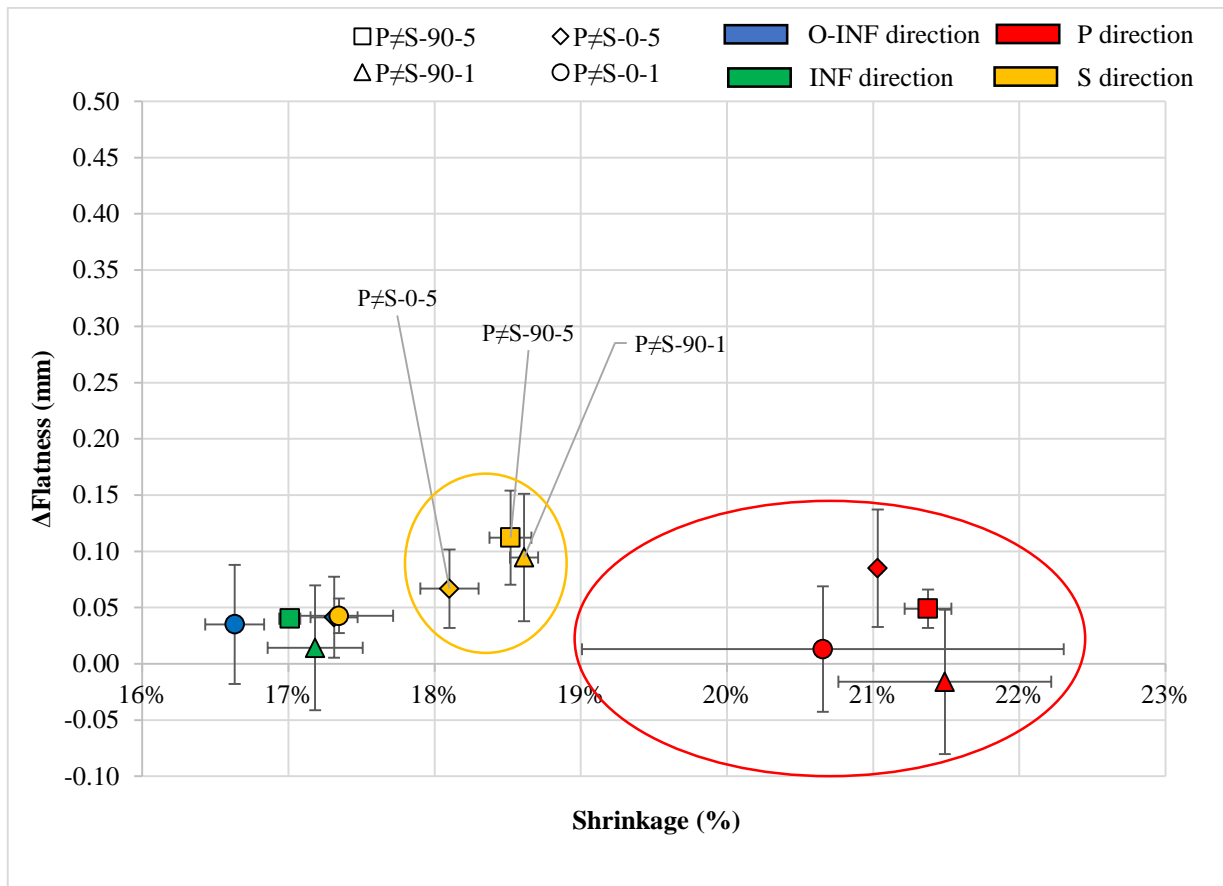**Fig. 16.** Comparison between flatness and shrinkage values for the P=S configuration.

Fig. 17. Comparison between flatness and shrinkage values for the P≠S configuration.

4. Conclusion

In this work, the shrinkage phenomenon occurring during the sintering phase of the metal MEX process chain was investigated on 17-4 PH samples, by varying printing and sintering orientation, infill line direction and aspect ratio. Among the obtained results, the condition where the sample orientation during printing was different from the orientation during sintering produced interesting and useful results. This condition is, indeed, very often required when complex geometries with high aspect ratio need to be realized or when the sample dimensions exceed one of the dimensions of the furnace. The main findings are reported as follows:

- When the configuration P=S is considered, the shrinkage was characterized by higher values along the printing/sintering direction, and it was higher for the parallelepipeds (higher aspect ratio).

- For what concerns the configuration P≠S, the highest shrinkage was observed along the printing direction, followed by the sintering direction. In this case, a higher shrinkage was observed when the shrinkage direction corresponded to the direction orthogonal to the infill line, while the aspect ratio was found to be not relevant in this condition.

The geometric accuracy, in terms of flatness values, was also investigated, and the obtained results highlighted that the flatness error increased when passing from green to sintered condition, showing a general worsening effect of the sintering on the geometric accuracy. This was most relevant when delamination defects occurred, while not a significant relation was found between the shrinkage and the increase of geometric errors, except for some isolated cases.

The results obtained can be considered as an important guideline to identify the right oversizing factor to obtain dimensions closer to the nominal ones, by considering two different scenarios (P=S and P≠S) as well as, different geometries and infill line strategies. A deeper knowledge about the shrinkage phenomenon is fundamental for the implementation of the metal MEX as a technology able to manufacture complex structures, such as lattices or gyroids based, ever more implemented in many industrial sectors.

Moreover, this study provided useful insights for further works focused on the comprehension of the entire process chain.

Declaration of competing interest

The authors declare that they have no known competing financial interests or personal relationships that could have appeared to influence the work reported in this paper.

Acknowledgments

5. References

[1]   G. Singh, J.M. Missiaen, D. Bouvard, J.M. Chaix, Copper additive manufacturing using MIM feedstock: adjustment of printing, debinding, and sintering parameters for processing dense and defectless parts, Int. J. Adv. Manuf. Technol. 115 (2021) 449–462. doi:10.1007/s00170-

021-07188-y.

[2]   M. Gabilondo, X. Cearsolo, M. Arrue, F. Castro, Influence of Build Orientation, Chamber Temperature and Infill Pattern on Mechanical Properties of 316L Parts Manufactured by Bound Metal Deposition, Materials (Basel). 15 (2022). doi:10.3390/ma15031183.

[3]   R. Huang, M. Riddle, D. Graziano, J. Warren, S. Das, S. Nimbalkar, J. Cresko, E. Masanet, Energy and emissions saving potential of additive manufacturing: the case of lightweight aircraft components, J. Clean. Prod. 135 (2016) 1559–1570. doi:10.1016/j.jclepro.2015.04.109.

[4]   D. Rejeski, F. Zhao, Y. Huang, Research needs and recommendations on environmental implications of additive manufacturing, Addit. Manuf. 19 (2018) 21–28. doi:10.1016/j.addma.2017.10.019.

[5]   G. Singh, Experimental investigations into mechanical and thermal properties of rapid manufactured copper parts, Proc IMechE Part C J Mech. Eng. Sci. 234 (2020) 82–95. doi:10.1177/0954406219875483.

[6]   M. Sadaf, M. Bragaglia, F. Nanni, A simple route for additive manufacturing of 316L stainless steel via Fused Filament Fabrication, J. Manuf. Process. 67 (2021) 141–150. doi:10.1016/j.jmapro.2021.04.055.

[7]   G. Wu, N.A. Langrana, R. Sadanji, S. Danforth, Solid freeform fabrication of metal components using fused deposition of metals, Mater. Des. 23 (2002) 97–105. doi:10.1016/s0261-3069(01)00079-6.

[8]   B. Liu, Y. Wang, Z. Lin, T. Zhang, Creating metal parts by Fused Deposition Modeling and Sintering, Mater. Lett. 263 (2020) 127252. doi:10.1016/j.matlet.2019.127252.

[9]   F. Lavecchia, A. Pellegrini, L.M. Galantucci, Comparative study on the properties of 17-4 PH stainless steel parts made by metal fused filament fabrication process and atomic diffusion additive manufacturing, Rapid Prototyp. J. 29 (2023) 393–407. doi:10.1108/RPJ-12-2021-0350.

[10]   J. Gonzalez-Gutierrez, S. Cano, S. Schuschnigg, C. Kukla, J. Sapkota, C. Holzer, Additive manufacturing of metallic and ceramic components by the material extrusion of highly-filled polymers: A review and future perspectives, Materials (Basel). 11 (2018). doi:10.3390/ma11050840.

[11] J. Gonzalez-Gutierrez, D. Godec, C. Kukla, T. Schlauf, C. Burkhardt, C. Holzer, Shaping , Debinding and Sintering of Steel Components Via Fused Filament Fabrication, 16th Int. Sci. Conf. Prod. Eng. - CIM2017. (2017) 99–104.

[12] P. Parenti, D. Puccio, B.M. Colosimo, Q. Semeraro, A new solution for assessing the printability of 17-4 PH gyroids produced via extrusion-based metal AM, J. Manuf. Process. 74 (2022) 557–572. doi:10.1016/j.jmapro.2021.12.043.

[13] F. Léonard, S. Tammas-Williams, Metal FFF sintering shrinkage rate measurements by X-ray computed tomography, Nondestruct. Test. Eval. 37 (2022) 631–644. doi:10.1080/10589759.2022.2085702.

[14] H.J. Sung, T.K. Ha, S. Ahn, Y.W. Chang, Powder injection molding of a 17-4 PH stainless steel and the effect of sintering temperature on its microstructure and mechanical properties, J. Mater. Process. Technol. 130–131 (2002) 321–327. doi:10.1016/S0924-0136(02)00739-2.

[15] G. Singh, J.M. Missiaen, D. Bouvard, J.M. Chaix, Additive manufacturing of 17–4 PH steel using metal injection molding feedstock: Analysis of 3D extrusion printing, debinding and sintering, Addit. Manuf. 47 (2021). doi:10.1016/j.addma.2021.102287.

[16] D.F. Heaney, R. Spina, Numerical analysis of debinding and sintering of MIM parts, J. Mater. Process. Technol. 191 (2007) 385–389. doi:10.1016/j.jmatprotec.2007.03.080.

[17] J. Gonzalez-Gutierrez, Y. Thompson, D. Handl, S. Cano, S. Schuschnigg, P. Felfer, C. Kukla, C. Holzer, C. Burkhardt, Powder content in powder extrusion moulding of tool steel : Dimensional stability , shrinkage and hardness, Mater. Lett. 283 (2021) 128909. doi:10.1016/j.matlet.2020.128909.

[18] M.S. Huang, H.C. Hsu, Influence of injection moulding and sintering parameters on properties of 316L MIM compact, Powder Metall. 54 (2011) 299–307. doi:10.1179/003258909X12502679013819.

[19] T. Kurose, Y. Abe, M.V.A. Santos, Y. Kanaya, A. Ishigami, S. Tanaka, H. Ito, Influence of the layer directions on the properties of 316l stainless steel parts fabricated through fused deposition of metals, Materials (Basel). 13 (2020). doi:10.3390/ma13112493.

[20] M.Á. Caminero, A. Romero, J.M. Chacón, P.J. Núñez, E. García-Plaza, G.P. Rodríguez, Additive manufacturing of 316L stainless-steel structures using fused filament fabrication technology: mechanical and geometric properties, Rapid Prototyp. J. 27 (2021) 583–591. doi:10.1108/RPJ-06-2020-0120.

[21] J. Gonzalez-Gutierrez, S. Cano, J.V. Ecker, M. Kitzmantel, F. Arbeiter, C. Kukla, C. Holzer, Bending Properties of Lightweight Copper Specimens with Different Infill Patterns Produced by Material Extrusion Additive Manufacturing , Solvent Debinding and Sintering, Appl. Sci. (2021). doi:https:// doi.org/10.3390/app11167262.

[22] I. Ait-Mansour, N. Kretzschmar, S. Chekurov, M. Salmi, J. Rech, Design-dependent shrinkage compensation modeling and mechanical property targeting of metal FFF, Prog. Addit. Manuf. 5 (2020) 51–57. doi:10.1007/s40964-020-00124-8.

[23] M.Á. Caminero, A.R. Gutiérrez, J.M. Chacòn, E. García-Plaza, P.J. Nunez, Effects of fused fi lament fabrication parameters on the manufacturing of 316L stainless-steel components : geometric and mechanical properties, Rapid Prototyp. J. (2022). doi:10.1108/RPJ-01-2022-0023.

[24] D. Jiang, F. Ning, Anisotropic deformation of 316L stainless steel overhang structures built by material extrusion based additive manufacturing, Addit. Manuf. 50 (2022) 102545. doi:10.1016/j.addma.2021.102545.

[25] M.G. Guerra, F. Lavecchia, G. Maggipinto, L.M. Galantucci, G.A. Longo, Measuring techniques suitable for verification and repairing of industrial components: A comparison among optical systems, CIRP J. Manuf. Sci. Technol. 27 (2019) 114–123. doi:10.1016/j.cirpj.2019.09.003.

[26] J. González-Gutiérrez, G.B. Stringari, I. Emri, Powder Injection Molding of Metal and Ceramic Parts, Some Critical Issues for Injection Molding, Some Crit. Issues Inject. Molding. (2012) 65–88. http://www.intechopen.com/books/some-critical-issues-for-injection-molding/powder- injection-molding-of-metal-and-ceramic-parts-.

[27] ASTM International, Standard Test Methods for Density of Compacted or Sintered Powder Metallurgy (PM) Products Using Archimedes' Principle, Astm B962-13. i (2013) 1–7. doi:10.1520/B0962-17.2.

[28] A. Pellegrini, M.E. Palmieri, M.G. Guerra, Evaluation of anisotropic mechanical behaviour of 316L parts realized by metal fused filament fabrication using digital image correlation, Int. J. Adv. Manuf. Technol. (2022). doi:10.1007/s00170-022-09303-z.

[29] S.O. Obadimu, K.I. Kourousis, Shrinkage behaviour of material extrusion steel 316L: influence of primary 3D printing parameters, Rapid Prototyp. J. 28 (2022) 92–101. doi:10.1108/rpj-07-2022-0224.

[30] M. Galati, P. Minetola, Analysis of density, roughness, and accuracy of the atomic diffusion additive manufacturing (ADAM) process for metal parts, Materials (Basel). 12 (2019). doi:10.3390/ma1224122.

Declaration of interests

☒ The authors declare that they have no known competing financial interests or personal relationships that could have appeared to influence the work reported in this paper.

☐The authors declare the following financial interests/personal relationships which may be considered as potential competing interests: